High activity of an affinity-matured ACE2 decoy against Omicron SARS-CoV-2 and pre-emergent coronaviruses

Running Title: ACE2 decoy maintains activity against emerging coronavirus variants

[1]Joshua J. Sims, [1]Sharon Lian, [1]Rosemary L. Meggersee, [1]Aradhana Kasimsetty, and [1]James M. Wilson*

[1]Gene Therapy Program, Department of Medicine, Perelman School of Medicine, University of Pennsylvania, Philadelphia, PA 19104, USA

*Corresponding author:

James M. Wilson, MD, PhD

Gene Therapy Program

Perelman School of Medicine

University of Pennsylvania

125 South 31st Street, Suite 1200

Philadelphia, PA 19104, USA

Phone: 215-573-9020; Fax: 215-494-5444

E-mail: wilsonjm@upenn.edu

Abstract

The viral genome of severe acute respiratory syndrome coronavirus 2 (SARS-CoV-2), particularly its cell-binding spike protein gene, has undergone rapid evolution during the coronavirus disease 2019 (COVID-19) pandemic. Variants including Omicron BA.1 and Omicron BA.2 now seriously threaten the efficacy of therapeutic monoclonal antibodies and vaccines that target the spike protein. Viral evolution over a much longer timescale has generated a wide range of genetically distinct *sarbecoviruses* in animal populations, including the pandemic viruses SARS-CoV-2 and SARS-CoV-1. The genetic diversity and widespread zoonotic potential of this group complicates current attempts to develop drugs in preparation for the next *sarbecovirus* pandemic. Receptor-based decoy inhibitors can target a wide range of viral strains with a common receptor and may have intrinsic resistance to escape mutant generation and antigenic drift. We previously generated an affinity-matured decoy inhibitor based on the receptor target of the SARS-CoV-2 spike protein, angiotensin-converting enzyme 2 (ACE2), and deployed it in a recombinant adeno-associated virus vector (rAAV) for intranasal delivery and passive prophylaxis against COVID-19. Here, we demonstrate the exceptional binding and neutralizing potency of this ACE2 decoy against SARS-CoV-2 variants including Omicron BA.1 and Omicron BA.2. Tight decoy binding tracks with human ACE2 binding of viral spike receptor-binding domains across diverse clades of coronaviruses. Furthermore, in a coronavirus that cannot bind human ACE2, a variant that acquired human ACE2 binding was bound by the decoy with nanomolar affinity. Considering these results, we discuss a strategy of decoy-based treatment and passive protection to mitigate the ongoing COVID-19 pandemic and future airway virus threats.

Author Summary

Viral sequences can change dramatically during pandemics lasting multiple years. Likewise, evolution over centuries has generated genetically diverse virus families posing similar threats to humans. This variation presents a challenge to drug development, in both the breadth of achievable protection against related groups of viruses and the durability of therapeutic agents or vaccines during extended outbreaks. This phenomenon has played out dramatically during the coronavirus disease 2019 (COVID-19) pandemic. The highly divergent Omicron variants of severe acute respiratory syndrome coronavirus 2 (SARS-CoV-2) have upended previous gains won by vaccine and monoclonal antibody development. Moreover, ecological surveys have increasingly revealed a broad class of SARS-CoV-2-like viruses in animals, each poised to cause a future human pandemic. Here, we evaluate an alternative to antibody-based protection and prevention—a decoy molecule based on the SARS-CoV-2 receptor. Our engineered decoy has proven resistant to SARS-CoV-2 evolution during the ongoing COVID-19 pandemic and can neutralize all variants of concern, including Omicron BA.1 and Omicron BA.2. Furthermore, the decoy binds tightly to a broad class of *sarbecoviruses* related to pandemic SARS-CoV-2 and SARS-CoV-1, indicating that receptor decoys offer advantages over monoclonal antibodies and may be deployed during the COVID-19 pandemic and future coronavirus outbreaks to prevent and treat severe illness.

1. Introduction

Monoclonal antibody therapeutics with the ability to bind the spike protein of severe acute respiratory syndrome coronavirus 2 (SARS-CoV-2) and prevent cell entry have been critical tools in managing the coronavirus disease 2019 (COVID-19) pandemic (1, 2). These drugs prevent hospitalizations when applied early in the course of infection (3) and can provide critical passive protection for vulnerable populations of immunocompromised patients who cannot mount a protective response to vaccines (4). However, monoclonals have proven susceptible to SARS-CoV-2 evolution (5). This susceptibility may arise because the spike epitopes most sensitive to neutralization have been under intense selection as the virus has made gains in transmissibility and its ability to evade human immunity (6). Detailed structural analyses have highlighted that the SARS-CoV-2 receptor-binding domain (RBD) is obscured from antibodies by a thick glycan coat that it is particularly evident when the RBD is in the downward conformation, enabling it to evade neutralization. Additionally, the mobility of the RBD between up and down conformations may itself present an issue for RBD:antibody interactions (7). Thus, monoclonal antibodies that target the RBD in the upward conformation may show reduced susceptibility (7, 8).

Several groups have identified several sites present in the functional binding epitope of the RBD spike protein that have undergone mutations to evade all currently available classes of monoclonal antibodies (9-11). The most significant escape mutants identified are K417 for class 1 antibodies, L452R and E484 for class 2 antibodies, and R346, K444, and G446-450 sites for class 3 antibodies (9, 11). It is concerning that many of these mutations are present in emergent

87 CoV-2 variants, which also show reduced susceptibility to monoclonal antibodies (9, 12, 13).
88 While comprehensive structural analysis suggests potential improvements for targeting
89 monoclonal antibodies and other biologics to the spike protein for inhibition (14-17), the fact
90 remains that SARS-CoV-2 evolution during the course of the pandemic has generated variants
91 which have evaded essentially the whole spectrum of clinical monoclonal candidates to date (5,
92 18). Furthermore, evidence suggests that application of single monoclonal antibody types in a
93 therapeutic setting can rapidly give rise to escape mutants (19-22). Together, these findings call
94 into question the ability of the antibody platform to keep pace with the course of the COVID-19
95 pandemic, or to be of use in future pandemics caused by other coronaviruses.

96

97 Receptor decoys may represent a mode of viral neutralization that is more resistant to continued
98 viral evolution and escape-mutant generation (23). SARS-CoV-2 evolution has occurred in a
99 way that retains tight binding to its primary cell entry receptor, angiotensin-converting enzyme 2
100 (ACE2) (24). We and others have developed affinity-matured, soluble ACE2 decoy molecules
101 that potently neutralize SARS-CoV-2 (23, 25-30). Our soluble Fc-fused decoy, CDY14HL-Fc4,
102 contains six amino acid substitutions that improve the neutralization of CoV-2 variants by 300-
103 fold versus un-engineered ACE2 and an active site mutation that ablates its endogenous
104 angiotensin-cleaving activity. Furthermore, CDY14HL maintains tight binding or neutralizing
105 activity for the distantly related betacoronaviruses (*sarbecoviruses*) WIV1-CoV, and SARS-
106 CoV-1 despite being engineered for improved activity against SARS-CoV-2 (25). This property
107 suggests that this decoy may be a useful tool to combat future pandemics from currently pre-
108 emergent, ACE2-dependent coronaviruses.

109

110 Here, we evaluate the binding and neutralization activity of CDY14HL against a wide range of
111 emerging SARS-CoV-2 variants, including Omicron BA.1 and Omicron BA.2, and a wide range
112 of pre-emergent coronaviruses with similarity to SARS-CoV-1 and SARS-CoV-2. These studies
113 suggest the broad utility of decoy-based viral entry inhibitors in combating current and future
114 coronavirus pandemics.

115

116 **2. Results**

117 **2.1 CDY14HL maintains tight binding to diverse SARS-CoV-2 variants**

118 We set out to evaluate the ability of our engineered ACE2 decoy to neutralize emerging SARS-
119 CoV-2 strains. We previously assessed binding between the decoy and CoV RBDs by first
120 expressing and purifying the RBDs and subjecting these to binding analysis using surface
121 plasmon resonance (25). We sought an RBD binding assay that would allow us to assess a broad
122 range of viral sequences for decoy compatibility quickly, without the need to express and purify
123 unique viral proteins. As a first step, we assessed binding to variant RBDs using a yeast display
124 system (31) (**Figure 1A**). We generated budding yeast displaying viral RBDs as fusion proteins
125 to the cell-surface-tethered yeast protein Aga2. We then incubated the RBD yeast with
126 CDY14HL-Fc1 fusion protein and assessed decoy binding via flow cytometry by staining bound
127 decoy with a fluorescent secondary antibody. CDY14HL-Fc1 bound the ancestral (Wuhan-Hu-1)
128 RBD with an apparent affinity of 0.14 nM (**Figure 1B and Table 1**). This result is in good
129 agreement with the 0.21 nM affinity obtained for the interaction using an orthogonal technique,
130 bio-layer interferometry (BLI, **Figure S1**), as well as with the picomolar binding affinity we
131 previously measured for CDY14HL-Fc4:RBD interaction using surface plasmon resonance (25).

132

133 Since our first description of CDY14HL (25), several SARS-CoV-2 variants of concern (VoCs)
134 have emerged, some with greater transmissibility and clinical sequelae than the original Wuhan
135 strain (13, 32, 33); most of the RBD evolution has occurred at the ACE2 interface (**Figures 1C**
136 **and 1D**) and could impact decoy affinity. We used the yeast display system to evaluate decoy
137 binding to RBDs from five of these VoCs (Iota, Delta, Delta Plus, Lambda, and Mu). CDY14HL
138 maintained sub-nanomolar binding affinity for all VoC RBDs (**Figure 1B and Table 1**). This
139 finding is consistent with the broad resistance of CDY14HL to SARS-CoV-2 variant evolution
140 previously observed in binding and pseudotype neutralization studies (25).

141

142 Next, we examined the Omicron VoCs. Unlike previous variants, which contain one, two, or
143 three RBD mutations, the Omicron BA.1 RBD differs from the ancestral strain by 15 amino
144 acids (**Figure 1E**) (34), while the Omicron BA.2 variant RBD differs by 16 amino acids from the
145 ancestral strain (**Figure 1F**). This level of mutation has caused a reduction in the efficacy of
146 first-generation vaccines and most of the monoclonal antibodies developed for therapeutic and
147 passive prophylaxis applications (35-40). Since our decoy was engineered for optimal binding to
148 the ancestral strain, we sought to determine if this degree of antigenic drift would impact binding
149 to the Omicron strains. Remarkably, the CDY14HL-Fc1 bound both Omicron strain RBDs with
150 sub-nanomolar affinity as measured by the RBD yeast display assay (**Figure 1B** and **Table 1**).
151 The decoy bound yeast-displayed Omicron RBDs at least four-fold more tightly than the
152 ancestral RBD (0.03 nM and 0.02 nM for the BA.1 and BA.2 strains, respectively, **Table 1**).
153 Another group working on their own decoy recently tested CDY14HL-Fc1 using a similar
154 binding strategy, using HEK293 cells expressing Omicron BA.1 and BA.2 spike glycoprotein

155 instead of yeast. Their results corroborate our data and highlighted that our decoy bound
156 Omicron BA.1 and BA.2 at low nanomolar concentrations (18). We have also confirmed sub-
157 nanomolar decoy affinity for the Omicron strain RBDs using BLI, though the two distinct assay
158 formats produced different rank-orders of variant affinities (**Figure S1**).

159

160 **2.2 CDY14HL maintains potent neutralization for diverse SARS-CoV-2 variants**

161 We next investigated whether the broad decoy affinity for SARS-CoV-2 variants observed using
162 the yeast display binding assay would translate to potent viral neutralization. We used
163 lentiviruses harboring a luciferase reporter gene and pseudotyped with spike proteins from
164 various SARS-CoV-2 strains to measure the neutralization potency (half-maximal inhibitory
165 concentration [IC50]) of purified CDY14HL-Fc1 decoy . CDY14HL-Fc1 neutralized Omicron
166 BA.1 and BA.2 more potently than the ancestral strain (18 ng/ml for BA.1 and 30 ng/ml for
167 BA.2 vs. 35 ng/ml for Wuhan-Hu-1, **Figure 2 and Table 1**). We extended this approach to
168 include 6 additional variants (Delta, Delta Plus, Kappa, Lambda, Mu, and Zeta) . CDY14HL
169 neutralized all SARS-CoV-2 strain pseudotypes tested with IC50 values near or below the
170 potency of the ancestral strain, Wuhan, against which it was engineered (**Figure 2**). Together
171 with these binding data, these variant neutralization data indicate that the CDY14HL decoy has a
172 broad tolerance for CoV-2 strain evolution, losing virtually no potency in the face of extensive
173 viral spike remodeling under the evolutionary pressures of a several-year-long global pandemic.

174

175 **2.3 CDY14HL binds diverse ACE2-dependent CoVs**

176 Given the broad activity towards SARS-CoV-2 variants with diverse spike sequences, we next
177 evaluated the ability of CDY14HL to bind RBDs from a diverse set of coronaviruses with
178 pandemic potential. Aside from SARS-CoV-1 and SARS-CoV-2, we identified 23
179 *sarbecoviruses* isolated from bats across Asia, Africa, and Europe (24, 41-53), many of which
180 are thought to use ACE2 as a receptor (**Figure 3A**). We cloned synthetic RBD genes into the
181 yeast display format for binding analysis (**Table 2**). Additionally, we included the RBD from the
182 human coronavirus NL63, an alpha-CoV with a genetically distinct RBD that has been shown to
183 use ACE2 for cell entry (54). We determined the binding affinities of yeast-displayed RBD to
184 CDY14HL-Fc1 by flow cytometry.

185

186 Several patterns in decoy binding emerged. *Sarbecoviruses* from clades 1a and 1b (CoV-1-like
187 and CoV-2-like CoVs, respectively, isolated from southern China and Laos) bound CDY14HL
188 with sub-nanomolar affinities in the yeast display assay. The exception to this trend was
189 RaTG13, which had a dissociation equilibrium constant of 1.4 nM (**Table 2**). Research has
190 recently shown that RaTG13 has weaker binding to human ACE2 than other members of the
191 clade (55). This behavior suggests that affinity for the decoy and the endogenous human ACE2
192 receptor are closely linked, as we have previously observed (25).

193

194 Except for Khosta-2 (56), *sarbecoviruses* from clades 2 and 3 (isolated in Asia and
195 Europe/Africa, respectively) did not bind CDY14HL-Fc1. Based on a recent survey of
196 RBD:ACE2 usage (56), we suspected these clade 2 and 3 RBDs were not capable of human
197 ACE2 binding, which we confirmed in the yeast display system using a soluble wild-type human

198 ACE2-Fc1 fusion protein at 100 nM (**Figure 3B**). Interestingly, Bloom and colleagues recently
199 discovered that a K493Y/T498W double mutation to the RBD of the clade 3 CoV BtKY72
200 confers human ACE2 binding (56). We found that our decoy bound BtKY72 K493Y/T498W
201 RBD with sub-nanomolar affinity, though it could not bind wt-BtKY72 (**Table 2**, **Figure 3C**).
202 This suggests that if distant CoVs acquire mutations that confer the potential for zoonotic spread,
203 CDY14HL would retain potent inhibitory potential.

204

205 These binding data are in broad agreement with our previous work demonstrating tight decoy
206 binding to RBDs from SARS-CoV-1 and WIV1-CoV (25); indeed, we confirm SARS-CoV-1
207 and WIV1-CoV binding here using the yeast display assay (**Table 2**). However, we reasoned that
208 viral neutralization comes about not only due to the decoy affinity for the viral target, but also
209 from the ability of the decoy to compete for viral binding with the endogenous ACE2 receptor.
210 To assess this possibility, we employed a competitive binding assay between the decoy and
211 ACE2 receptor in the yeast system. We incubated RBD yeast with a low concentration of decoy
212 (1 nM of CDY14HL-hFc1; 95 ng/ml) along with a 100-fold molar excess of wt-ACE2 (100 nM
213 of wt-ACE2-mFc, with a mouse Fc fusion to distinguish it from the decoy). We assessed the
214 level of decoy binding retained in the presence of receptor competition by flow cytometry and
215 compared these values across the set of RBDs (**Figure 3D**).

216

217 The positive control, the RBD from the well-neutralized ancestral SARS-CoV-2 strain, retained
218 34% of decoy binding in the presence of 100-fold molar excess of wt-ACE2-mFc (**Figure 3E**).
219 Similar to SARS-CoV-2, all clade 1a and 1b *sarbecovirus* RBDs tested retained at least 24%

220 binding in the competition assay. Khosta-2, a clade 3 RBD with weak decoy binding (**Table 2**),
221 retained 79% percent decoy binding in the presence of 100-fold excess wt-ACE2. Similarly, the
222 relatively weak-binding RBD from RaTG13 also retained almost complete decoy binding under
223 competition. These examples highlight that decoy affinity alone may be a poor determinant of
224 the ability to compete with endogenous ACE2 as an inhibitor (**Figure S2**). The lone alpha-CoV
225 in our study, NL63, retained the lowest fraction of decoy binding in the competition assay (21%,
226 **Figure 3E**). Further study is needed to determine whether this result indicates a lower
227 neutralizing potency of the decoy for the genetically distinct ACE2-dependent alpha-CoVs.
228 Together with the observed sub-nanomolar decoy binding affinity, these competitive binding
229 data predict broad and potent neutralization of beta-CoVs that can bind human ACE2. As many
230 factors including subtle shifts in co-receptor usage and cell entry mechanism can define the
231 potency of an inhibitor (57), further studies with diverse CoVs in pseudotyped and live-virus
232 systems will be required to confirm this finding.

233

234 **3. Discussion**

235 Currently available COVID-19 treatments such as monoclonal antibodies are fast becoming less
236 effective as new variants emerge (12, 58). Alternative protein-based viral neutralizers exist,
237 including camelid-derived single chain antibodies. While these have several advantages over
238 conventional antibodies with respect to small size, delivery modalities, and manufacturability
239 (59-61), nanobodies still recognize a specific epitope on the SARS-CoV-2 RBD spike surface
240 and thus are still susceptible to mutations that could eliminate this binding epitope.

241

242 We previously reported the development of an affinity-matured, soluble ACE2 decoy, termed
243 CDY14HL. This decoy binds and neutralizes SARS-CoV-2 strains from the early pandemic as
244 well as the related pandemic *sarbecovirus*, SARS-CoV-1 (25). In this study, we have shown that
245 the affinity-matured decoy retains broad neutralizing activity against every SARS-CoV-2 variant
246 tested, including Delta, Delta Plus, Omicron BA.1, and Omicron BA.2. These results highlight a
247 major advantage of receptor-based decoy molecules over other viral spike inhibitor biologics;
248 unlike monoclonal antibodies, decoy binding of a variant is tightly linked to receptor binding and
249 thus viral fitness through evolution. Zhang *et al*., illustrated this very effectively through their
250 own affinity experiments where they compared engineered decoy binding of omicron BA.1 and
251 BA.2 to four monoclonal antibodies authorized for clinical use (18). They determined that
252 REGN10933 and LY-CoV555 had no binding activity to either Omicron BA.1 or BA.2.
253 REGN10987 was found to bind to Omicron BA.2 weakly and Omicron BA.1 not at all.
254 However, the most surprising result was for VIR-7831, a monoclonal targeting a distinct and
255 highly conserved spike site that was selected to yield both broad sarbecovirus neutralization and
256 resistance to SARS-CoV-2 variant evolution (62). VIR-7831 was only able to bind to Omicron
257 BA.1 and very weakly to BA.2, a fact that subsequently led to the removal of FDA authorization
258 for the drug (63).

259

260 Our original strategy for deploying the decoy was developed in the context of preventing SARS-
261 CoV-2 infection. We accomplished this aim through the creation of a recombinant adeno-
262 associated virus (rAAV) vector expressing the decoy that is administered nasally to engineer
263 proximal airway cells to express neutralizing levels of the decoy at the airway surface (i.e., the
264 virus's entry point). This approach could be particularly useful for immunocompromised patients

265 who do not generate protective immunity following active vaccination. We are also developing
266 the decoy as a therapeutic protein for treatment, or possibly prevention in high-risk groups,
267 following parenteral administration.

268 The relentless emergence of new, highly transmissible SARS-CoV-2 variants in the current
269 pandemic reminds us of our vulnerability to the power of zoonosis and the intense selection
270 pressures experienced by pandemic viruses to evolve into more pathogenic and/or transmissible
271 variants. This experience suggests the importance of proactively developing countermeasures
272 against future pandemics, which will likely be caused by a coronavirus based on the recent
273 history of SARS, Middle East respiratory syndrome, and COVID-19. Indeed, CoVs constitute a
274 major fraction of pre-zoonotic viruses ranked by multiple genetic and environmental factors for
275 pandemic potential (64). This threat compelled us to evaluate the competitive binding of our
276 ACE2 decoy to spike proteins from a variety of animal coronaviruses with zoonotic potential,
277 particularly *sarbecoviruses* that can bind human ACE2, or that whose viral spike proteins only
278 need a small number of mutations to acquire human ACE2 binding. We were delighted to find
279 that the decoy retained very high binding activity against spike proteins from every pre-emergent
280 strain studied that also had the ability to bind human ACE2, suggesting the broad utility of the
281 decoy in the current and future coronavirus pandemics.

282

283 COVID-19 has illustrated how powerful the drive for viral fitness can be in circumventing
284 immunity generated from previous infection, vaccines, and antibody therapeutics. This rapid
285 evolution is substantially amplified in the setting of a global pandemic caused by a highly
286 transmissible virus. The use of a decoy protein based on a soluble version of a viral receptor
287 holds the promise of significantly restricting viral escape, as any mutation that diminishes decoy

288 binding will likely also diminish receptor binding and thus viral fitness. We are quickly moving
289 this ACE2 decoy into the clinic in the AAV platform as well as a protein therapeutic as a
290 possible solution to COVID-19 variants and to prepare for future coronavirus outbreaks.

291

292

293

294

295

296

297

298

299

300

301

302

303

304

305

306

307 **Tables**

308 **Table 1:** RBD binding constants and neutralization IC50 values for CDY14HL-Fc1 vs SARS-

309 CoV-2 variants

Strain	RBD mutations relative to Wuhan-Hu1	Yeast assay RBD binding K_D (nM)	Pseudotype neutralization assay IC50 (ng/ml)
CoV-2 (Wuhan-Hu-1)	none	0.14	35
Delta	L452R T478K	0.21	14
Delta Plus	K417N L452R T478K	0.21	10
Delta with 439K/484K/501Y	K417N N439K L452R T478K E484K N501Y	0.07	NC
Iota	E484K	0.10	NC
Kappa	L452R E484Q	NC	18
Lambda	L452Q F490S	0.20	11
Mu	R346K E484K N501Y	0.10	21
Omicron BA.1	G339D S371L S373P S375F K417N N440K G446S S477N T478K E484A Q493K G496S Q498R N501Y Y505H	0.031	18
Omicron BA.2	G339D S371F S373P S375F T376A D405N R408S K417N N440K S477N T478K E484A Q493R Q498R N501Y Y505H	0.024	30
Zeta	E484K	NC	37

310

311 NC: Not Collected

312

313

314

315

316

317 **Table 2:** *Sarbecovirus* RBD sequence and decoy binding data

	Virus	Genome	Spike protein	RBD amino acids	K_D (nM)
	NL63	AY567487.2	AAS58177.1	481-614	0.22
Clade 1a	CoV-1 (Urbani)	AY278741.1	AAP13441.1	317-569	0.25
	LYRa11	KF569996.1	AHX37558.1	321-520	0.29
	Rs3367	KC881006.1	AGZ48818.1	318-570	0.19
	Rs4048	KY417144.1	ATO98132.1	318-517	0.31
	Rs4231	KY417146.1	ATO98157.1	317-516	0.30
	Rs4874	KY417150.1	ATO98205.1	317-516	0.23
	Rs7327	KY417151.1	ATO98218.1	318-517	0.31
	RsSHC014	KC881005.1	AGZ48806.1	318-517	0.31
	WIV1	KF367457.1	AGZ48831.1	318-570	0.20
	WIV16	KT444582.1	ALK02457.1	318-510	0.24
Clade 1b	BANAL-103	MZ937001.1	UAY13229.1	326-526	0.30
	BANAL-236	MZ937003.2	UAY13253.1	326-526	0.24
	CoV-2 (Wuhan-Hu-1)	NC_045512.2	YP_009724390.1	330-530	0.14
	RaTG13	MN996532.2	QHR63300.2	319-542	1.40
Clade 2	16BO133	KY938558.1	ASO66810.1	317-549	NB
	Anlong-112	KY770859.1	ARI44804.1	314-547	NB
	As6526	KY417142.1	ATO98108.1	322-554	NB
	Rf4092	KY417145.1	ATO98145.1	315-548	NB
	Rs4255	KY417149.1	ATO98193.1	322-554	NB
	ZC45	MG772933.1	AVP78031.1	327-560	NB
	ZCX21	MG772934.1	AVP78042.1	326-559	NB
Clade 3	BM48-31	GU190215.1	ADK66841.1	321-570	NB
	BtKY72	KY352407.1	APO40579.1	320-519	NB
	BtKY72 K493Y/T498W	*	*	*	0.26
	Khosta-1	MZ190137.1	QVN46559.1	309-528	NB
	Khosta-2	MZ190138.1	QVN46569.1	307-526	1.90

318

319 *BtKY72 K493Y/T498W RBD is based on wt with mutations at BtKY72 spike residue 482/487

320 (56).

321 NB = No Binding detected at 100 nM decoy

322

323 **4. Materials and Methods**

324 **4.1 CoV pseudotyped lentiviral neutralization assay**

325 **4.1 CoV pseudotyped lentiviral neutralization assay**

326 Replication-incompetent lentiviruses pseudotyped with full-length CoV spike proteins and
327 packaging for a Renilla luciferase reporter gene were purchased from Integral Molecular: RVP-
328 701L Wuhan (lot CL-114B), RVP-763L Delta (lot CL-267A), RVP-736L Zeta (lot CL-255A),
329 RVP-730L Kappa (lot CL-247A), RVP-768L Omicron BA.1 (lot CL-297A), RVP-770L
330 Omicron BA.2 (lot CL-310), RVP-767L Mu (lot CL-274A), RVP-766L Lambda (lot CL-259A),
331 and RVP-765L Delta Plus (lot CL-258A). They have been shown to be suitable for neutralization
332 measurements with a high linear correlation of IC50s measured by the pseudotyped virus
333 neutralization assay with SARS-CoV-2 PRNT (65). We performed neutralization assays using
334 human embryonic kidney 293T cells overexpressing ACE2 (Integral Molecular) as previously
335 described (25), performing a minimum of 3 replicates to arrive at the data presented.

336

337 **4.2 Recombinant protein production**

338 To generate wt-ACE2-mFc for competitive binding assays, we cloned human ACE2 (1–615)
339 fused to a C-terminal mouse IgG2a Fc into pcDNA3.1. We transfected the plasmid into Expi293
340 cells for expression. The supernatant was collected and exchanged to 0.1 M sodium
341 phosphate, pH 7.2 and 150 mM NaCl buffer for purification on Protein A Sepharose 4B
342 (ThermoFisher). The protein was eluted in 0.1 M citric acid, pH 3.0 and neutralized in 1 M Tris,
343 pH 9.0 before a final buffer exchange to 25 mM HEPES pH 7.2 and 150 mM NaCl by size-
344 exclusion chromatography with Superose 6 resin (Cytiva). For these studies, we cloned the
345 engineered CDY14HL 1–615 fragment in front of the human IgG1 Fc domain for expression and

346 purification. We previously characterized a decoy fusion to human IgG4 Fc (25), but found that
347 Fc1 and Fc4 decoy fusions behave similarly with respect to binding and neutralization (e.g., the
348 IC50 values against Wuhan-Hu1 pseudotypes were 37 ng/ml and 35 ng/ml for CDY14HL-Fc4
349 and CDY14HL-Fc1, respectively).
350

351 **4.3 Phylogenic tree construction**

352 The RBD sequences of the CoVs were taken from spike protein coding sequences (**Table 2**)
353 downloaded from the National Center for Biotechnology Information (NCBI). Using MEGA X
354 (66), we aligned the amino acid sequences in ClustalW and constructed a phylogenic tree using
355 maximum likelihood analysis and bootstrapping with 100 replicates.
356

357 **4.4 Yeast display binding assays**

358 The nucleic acid sequences of the CoV RBDs were taken from NCBI. Accession numbers and
359 domain boundary details are included in **Table 2**.We cloned the RBDs into a plasmid between an
360 upstream yeast Aga2 gene and a downstream hemagglutinin (HA) epitope tag with flexible GSG
361 linkers. The plasmid has a low-copy centromeric origin similar to that of pTCON2 (67).
362 Plasmids were transformed into EBY100 using the Frozen-EZ Yeast Transformation II Kit
363 (Zymo). We grew colonies in SD-Trp media before induction in log phase for 24 hr at 30˚C in
364 SG-CAA (67). To determine K_D, yeast were incubated with a 1:10 dilution series of CDY14HL-
365 Fc1 for 16 hr at 25˚C. To check for ACE2 binding, yeast were incubated with 100 nM of
366 CDY14HL-Fc1 or wt-ACE2-mFc for 16 hr at 25˚C. For the competition binding, yeast were
367 incubated with 1 nM of CDY14HL-Fc1 and 100 nM of wt-ACE2-mFc for 30 min at 25˚C.
368 Afterwards, samples were washed and stained for flow cytometry using appropriate seconday

369 antibodies: goat anti-human fluorescein isothiocyanate (FITC; ThermoFisher A18812), anti-
370 mouse Alexa Fluor 488 (Cell Signaling Technology 4408S), or rabbit anti-HA-PE (Cell
371 Signaling Technology 14904S). We used phosphate-buffered saline with 0.1% bovine serum
372 albumin for all staining and washes. For the titration of CDY14HL-Fc1, we incubated the yeast
373 with 1:10 dilution series of CDY14HL-Fc1 at 25˚C for 6 hr. The yeast were analyzed on an
374 ACEA NovoCyte flow cytometer. We determined the level of CDY14HL-Fc1 binding by taking
375 the mean FITC signal for 500 RBD+ yeast cells collected for each condition. We collected a
376 minimum of 4 replicate binding curves to establish dissociation constants for each RBD variant.
377 Since different RBDs expressed to slightly different levels on the surface of the yeast, for the
378 purposes of plotting multiple binding curves in the same figure we normalized bound decoy
379 fluorescence for each curve to its fit maximum value. We fitted the decoy concentration versus
380 the decoy binding signal in GraphPad Prism using a three-parameter fit to the binding isotherm.
381
382
383
384
385
386
387
388
389

Data Availability Statement

All relevant data are within the manuscript.

Ethics Statement

N/A - IRB approval nor ethics approval were required as no medical samples, records, or animals were utilized in this study

Acknowledgments

We thank Henry Hoff, Adam Salazar, Simin Zaidi, Kenneth Yancey, Dmitriy Fedorenko, Jasmine Tan, Yida He, Philip McGurk, and Sai Prasad Ganesh for protein expression and purification in support of these studies. We thank Alex Martino for assistance with BLI studies. We thank Nathan Denton for assistance with manuscript preparation and graphics.

Author Contributions

J.J.S. – conceptualization, data curation, formal analysis, investigation, methodology, project administration, resources, supervision, validation, visualization, writing-original, writing-review, and edits. S.L. – conceptualization, data curation, formal analysis, investigation, methodology, resources, validation, visualization, writing-original, writing-review, and edits. R.M. data curation, formal analysis, investigation, project administration, visualization, writing-original,

writing-review, and edits. A.K. formal analysis, investigation, visualization, writing-original, writing-review, and edits J.M.W. – conceptualization, funding acquisition, writing-original, writing-review, and edits.

Funding

This work was funded by G2 Bio (recipient – J.M.W.). The funders had no role in study design, data collection and analysis, decision to publish, or preparation of the manuscript.

429 **Conflict of Interest Statement**

430 I have read the journal's policy and the authors of this manuscript have the following competing
431 interests: J.M.W. is a paid advisor to and holds equity in Scout Bio and Passage Bio. He also
432 holds equity in the G2 Bio-associated asset companies and iECURE. He has sponsored research
433 agreements with Amicus Therapeutics, Biogen, Elaaj Bio, FA212, G2 Bio, G2 Bio-associated
434 asset companies, iECURE, Janssen, Passage Bio, and Scout Bio, which are licensees of
435 University of Pennsylvania technology. J.M.W. and J.J.S. are inventors on patents/patents filed
436 by the University of Pennsylvania.

437

438

439

440

441

442

443

444

445

446

447

448

449 **References**

450 1. Wec AZ, Wrapp D, Herbert AS, Maurer DP, Haslwanter D, Sakharkar M, et al. Broad
451 neutralization of SARS-related viruses by human monoclonal antibodies. Science. 2020;369(6504):731-6.
452 2. Weinreich DM, Sivapalasingam S, Norton T, Ali S, Gao H, Bhore R, et al. REGN-COV2, a
453 Neutralizing Antibody Cocktail, in Outpatients with Covid-19. N Engl J Med. 2021;384(3):238-51.
454 3. Weinreich DM, Sivapalasingam S, Norton T, Ali S, Gao H, Bhore R, et al. REGEN-COV Antibody
455 Combination and Outcomes in Outpatients with Covid-19. N Engl J Med. 2021;385(23):e81.
456 4. O'Brien MP, Hou P, Weinreich DM. Subcutaneous REGEN-COV Antibody Combination to Prevent
457 Covid-19. Reply. N Engl J Med. 2021;385(20):e70.
458 5. Starr TN, Greaney AJ, Addetia A, Hannon WW, Choudhary MC, Dingens AS, et al. Prospective
459 mapping of viral mutations that escape antibodies used to treat COVID-19. Science.
460 2021;371(6531):850-4.
461 6. Barton MI, MacGowan SA, Kutuzov MA, Dushek O, Barton GJ, van der Merwe PA. Effects of
462 common mutations in the SARS-CoV-2 Spike RBD and its ligand, the human ACE2 receptor on binding
463 affinity and kinetics. Elife. 2021;10.
464 7. Turonova B, Sikora M, Schurmann C, Hagen WJH, Welsch S, Blanc FEC, et al. In situ structural
465 analysis of SARS-CoV-2 spike reveals flexibility mediated by three hinges. Science. 2020;370(6513):203-
466 8.
467 8. Pierri CL. SARS-CoV-2 spike protein: flexibility as a new target for fighting infection. Signal
468 Transduct Target Ther. 2020;5(1):254.
469 9. Ding C, He J, Zhang X, Jiang C, Sun Y, Zhang Y, et al. Crucial Mutations of Spike Protein on SARS-
470 CoV-2 Evolved to Variant Strains Escaping Neutralization of Convalescent Plasmas and RBD-Specific
471 Monoclonal Antibodies. Front Immunol. 2021;12:693775.
472 10. Greaney AJ, Loes AN, Crawford KHD, Starr TN, Malone KD, Chu HY, et al. Comprehensive
473 mapping of mutations in the SARS-CoV-2 receptor-binding domain that affect recognition by polyclonal
474 human plasma antibodies. Cell Host Microbe. 2021;29(3):463-76 e6.
475 11. Greaney AJ, Starr TN, Barnes CO, Weisblum Y, Schmidt F, Caskey M, et al. Mapping mutations to
476 the SARS-CoV-2 RBD that escape binding by different classes of antibodies. Nat Commun.
477 2021;12(1):4196.
478 12. Zhou H, Tada T, Dcosta BM, Landau NR. Neutralization of SARS-CoV-2 Omicron BA.2 by
479 Therapeutic Monoclonal Antibodies. bioRxiv. 2022.
480 13. Campbell F, Archer B, Laurenson-Schafer H, Jinnai Y, Konings F, Batra N, et al. Increased
481 transmissibility and global spread of SARS-CoV-2 variants of concern as at June 2021. Euro Surveill.
482 2021;26(24).
483 14. Mercurio I, Tragni V, Busto F, De Grassi A, Pierri CL. Protein structure analysis of the interactions
484 between SARS-CoV-2 spike protein and the human ACE2 receptor: from conformational changes to
485 novel neutralizing antibodies. Cell Mol Life Sci. 2021;78(4):1501-22.
486 15. Starr TN, Czudnochowski N, Liu Z, Zatta F, Park YJ, Addetia A, et al. SARS-CoV-2 RBD antibodies
487 that maximize breadth and resistance to escape. Nature. 2021;597(7874):97-102.
488 16. Walls AC, Park YJ, Tortorici MA, Wall A, McGuire AT, Veesler D. Structure, Function, and
489 Antigenicity of the SARS-CoV-2 Spike Glycoprotein. Cell. 2020;181(2):281-92 e6.
490 17. Wrapp D, Wang N, Corbett KS, Goldsmith JA, Hsieh CL, Abiona O, et al. Cryo-EM structure of the
491 2019-nCoV spike in the prefusion conformation. Science. 2020;367(6483):1260-3.
492 18. Zhang L, Narayanan KK, Cooper L, Chan KK, Devlin CA, Aguhob A, et al. An engineered ACE2
493 decoy receptor can be administered by inhalation and potently targets the BA.1 and BA.2 omicron
494 variants of SARS-CoV-2. bioRxiv. 2022.

495 19. Van Egeren D, Novokhodko A, Stoddard M, Tran U, Zetter B, Rogers M, et al. Risk of rapid
496 evolutionary escape from biomedical interventions targeting SARS-CoV-2 spike protein. PLoS One.
497 2021;16(4):e0250780.
498 20. Fenaux H, Gueneau R, Chaghouri A, Henry B, Mouna L, Roque-Afonso AM, et al. Emergence of
499 SARS-CoV-2 resistance mutations in a patient who received anti-SARS-COV2 spike protein monoclonal
500 antibodies: a case report. BMC Infect Dis. 2021;21(1):1223.
501 21. Jensen B, Luebke N, Feldt T, Keitel V, Brandenburger T, Kindgen-Milles D, et al. Emergence of the
502 E484K mutation in SARS-COV-2-infected immunocompromised patients treated with bamlanivimab in
503 Germany. Lancet Reg Health Eur. 2021;8:100164.
504 22. Rockett RJ, Basile K, Maddocks S, Fong W, Agius JE, Mackinnon JJ, et al. RESISTANCE
505 CONFERRING MUTATIONS IN SARS-CoV-2 DELTA FOLLOWING SOTROVIMAB INFUSION. medRxiv.
506 2021:2021.12.18.21267628.
507 23. Higuchi Y, Suzuki T, Arimori T, Ikemura N, Mihara E, Kirita Y, et al. Engineered ACE2 receptor
508 therapy overcomes mutational escape of SARS-CoV-2. Nat Commun. 2021;12(1):3802.
509 24. Letko M, Marzi A, Munster V. Functional assessment of cell entry and receptor usage for SARS-
510 CoV-2 and other lineage B betacoronaviruses. Nat Microbiol. 2020;5(4):562-9.
511 25. Sims JJ, Greig JA, Michalson KT, Lian S, Martino RA, Meggersee R, et al. Intranasal gene therapy
512 to prevent infection by SARS-CoV-2 variants. PLoS Pathog. 2021;17(7):e1009544.
513 26. Chan KK, Tan TJC, Narayanan KK, Procko E. An engineered decoy receptor for SARS-CoV-2
514 broadly binds protein S sequence variants. Sci Adv. 2021;7(8).
515 27. Glasgow A, Glasgow J, Limonta D, Solomon P, Lui I, Zhang Y, et al. Engineered ACE2 receptor
516 traps potently neutralize SARS-CoV-2. Proc Natl Acad Sci U S A. 2020;117(45):28046-55.
517 28. Havranek B, Chan KK, Wu A, Procko E, Islam SM. Computationally Designed ACE2 Decoy
518 Receptor Binds SARS-CoV-2 Spike (S) Protein with Tight Nanomolar Affinity. J Chem Inf Model.
519 2021;61(9):4656-69.
520 29. Jing W, Procko E. ACE2-based decoy receptors for SARS coronavirus 2. Proteins.
521 2021;89(9):1065-78.
522 30. Chan KK, Dorosky D, Sharma P, Abbasi SA, Dye JM, Kranz DM, et al. Engineering human ACE2 to
523 optimize binding to the spike protein of SARS coronavirus 2. Science. 2020;369(6508):1261-5.
524 31. Angelini A, Chen TF, de Picciotto S, Yang NJ, Tzeng A, Santos MS, et al. Protein Engineering and
525 Selection Using Yeast Surface Display. Methods Mol Biol. 2015;1319:3-36.
526 32. Ren SY, Wang WB, Gao RD, Zhou AM. Omicron variant (B.1.1.529) of SARS-CoV-2: Mutation,
527 infectivity, transmission, and vaccine resistance. World J Clin Cases. 2022;10(1):1-11.
528 33. Araf Y, Akter F, Tang YD, Fatemi R, Parvez MSA, Zheng C, et al. Omicron variant of SARS-CoV-2:
529 Genomics, transmissibility, and responses to current COVID-19 vaccines. J Med Virol. 2022;94(5):1825-
530 32.
531 34. Miller NL, Clark T, Raman R, Sasisekharan R. Insights on the mutational landscape of the SARS-
532 CoV-2 Omicron variant. bioRxiv. 2021.
533 35. Wilhelm A, Widera M, Grikscheit K, Toptan T, Schenk B, Pallas C, et al. Reduced Neutralization of
534 SARS-CoV-2 Omicron Variant by Vaccine Sera and Monoclonal Antibodies. medRxiv.
535 2021:2021.12.07.21267432.
536 36. Cao Y, Wang J, Jian F, Xiao T, Song W, Yisimayi A, et al. Omicron escapes the majority of existing
537 SARS-CoV-2 neutralizing antibodies. Nature. 2021.
538 37. Cameroni E, Bowen JE, Rosen LE, Saliba C, Zepeda SK, Culap K, et al. Broadly neutralizing
539 antibodies overcome SARS-CoV-2 Omicron antigenic shift. Nature. 2021.
540 38. Dejnirattisai W, Huo J, Zhou D, Zahradnik J, Supasa P, Liu C, et al. Omicron-B.1.1.529 leads to
541 widespread escape from neutralizing antibody responses. bioRxiv. 2021.

542 39. VanBlargan L, Errico J, Halfmann P, Zost S, Crowe J, Purcell L, et al. An infectious SARS-CoV-2
543 B.1.1.529 Omicron virus escapes neutralization by therapeutic monoclonal antibodies. Res Sq. 2021.
544 40. Dejnirattisai W, Shaw RH, Supasa P, Liu C, Stuart AS, Pollard AJ, et al. Reduced neutralisation of
545 SARS-CoV-2 omicron B.1.1.529 variant by post-immunisation serum. Lancet. 2022;399(10321):234-6.
546 41. Islam A, Ferdous J, Sayeed MA, Islam S, Kaisar Rahman M, Abedin J, et al. Spatial epidemiology
547 and genetic diversity of SARS-CoV-2 and related coronaviruses in domestic and wild animals. PLoS One.
548 2021;16(12):e0260635.
549 42. Temmam S, Vongphayloth K, Baquero E, Munier S, Bonomi M, Regnault B, et al. Bat
550 coronaviruses related to SARS-CoV-2 and infectious for human cells. Nature. 2022.
551 43. He B, Zhang Y, Xu L, Yang W, Yang F, Feng Y, et al. Identification of diverse alphacoronaviruses
552 and genomic characterization of a novel severe acute respiratory syndrome-like coronavirus from bats in
553 China. J Virol. 2014;88(12):7070-82.
554 44. Hu B, Zeng LP, Yang XL, Ge XY, Zhang W, Li B, et al. Discovery of a rich gene pool of bat SARS-
555 related coronaviruses provides new insights into the origin of SARS coronavirus. PLoS Pathog.
556 2017;13(11):e1006698.
557 45. Ge XY, Li JL, Yang XL, Chmura AA, Zhu G, Epstein JH, et al. Isolation and characterization of a bat
558 SARS-like coronavirus that uses the ACE2 receptor. Nature. 2013;503(7477):535-8.
559 46. Yang XL, Hu B, Wang B, Wang MN, Zhang Q, Zhang W, et al. Isolation and Characterization of a
560 Novel Bat Coronavirus Closely Related to the Direct Progenitor of Severe Acute Respiratory Syndrome
561 Coronavirus. J Virol. 2015;90(6):3253-6.
562 47. Zhou P, Yang XL, Wang XG, Hu B, Zhang L, Zhang W, et al. Addendum: A pneumonia outbreak
563 associated with a new coronavirus of probable bat origin. Nature. 2020;588(7836):E6.
564 48. Tao Y, Tong S. Complete Genome Sequence of a Severe Acute Respiratory Syndrome-Related
565 Coronavirus from Kenyan Bats. Microbiol Resour Announc. 2019;8(28).
566 49. Drexler JF, Gloza-Rausch F, Glende J, Corman VM, Muth D, Goettsche M, et al. Genomic
567 characterization of severe acute respiratory syndrome-related coronavirus in European bats and
568 classification of coronaviruses based on partial RNA-dependent RNA polymerase gene sequences. J Virol.
569 2010;84(21):11336-49.
570 50. Hu D, Zhu C, Ai L, He T, Wang Y, Ye F, et al. Genomic characterization and infectivity of a novel
571 SARS-like coronavirus in Chinese bats. Emerg Microbes Infect. 2018;7(1):154.
572 51. Kim Y, Son K, Kim YS, Lee SY, Jheong W, Oem JK. Complete genome analysis of a SARS-like bat
573 coronavirus identified in the Republic of Korea. Virus Genes. 2019;55(4):545-9.
574 52. Lin XD, Wang W, Hao ZY, Wang ZX, Guo WP, Guan XQ, et al. Extensive diversity of coronaviruses
575 in bats from China. Virology. 2017;507:1-10.
576 53. Alkhovsky S, Lenshin S, Romashin A, Vishnevskaya T, Vyshemirsky O, Bulycheva Y, et al. SARS-like
577 Coronaviruses in Horseshoe Bats (Rhinolophus spp.) in Russia, 2020. Viruses. 2022;14(1).
578 54. Hofmann H, Pyrc K, van der Hoek L, Geier M, Berkhout B, Pohlmann S. Human coronavirus NL63
579 employs the severe acute respiratory syndrome coronavirus receptor for cellular entry. Proc Natl Acad
580 Sci U S A. 2005;102(22):7988-93.
581 55. Wrobel AG, Benton DJ, Xu P, Roustan C, Martin SR, Rosenthal PB, et al. Author Correction: SARS-
582 CoV-2 and bat RaTG13 spike glycoprotein structures inform on virus evolution and furin-cleavage
583 effects. Nat Struct Mol Biol. 2020;27(10):1001.
584 56. Starr TN, Zepeda SK, Walls AC, Greaney AJ, Alkhovsky S, Veesler D, et al. ACE2 binding is an
585 ancestral and evolvable trait of sarbecoviruses. Nature. 2022;603(7903):913-8.
586 57. Singh M, Bansal V, Feschotte C. A Single-Cell RNA Expression Map of Human Coronavirus Entry
587 Factors. Cell Rep. 2020;32(12):108175.

588 58. VanBlargan LA, Errico JM, Halfmann PJ, Zost SJ, Crowe JE, Jr., Purcell LA, et al. An infectious
589 SARS-CoV-2 B.1.1.529 Omicron virus escapes neutralization by therapeutic monoclonal antibodies. Nat
590 Med. 2022;28(3):490-5.
591 59. Sasisekharan R. Preparing for the Future - Nanobodies for Covid-19? N Engl J Med.
592 2021;384(16):1568-71.
593 60. Huo J, Mikolajek H, Le Bas A, Clark JJ, Sharma P, Kipar A, et al. A potent SARS-CoV-2 neutralising
594 nanobody shows therapeutic efficacy in the Syrian golden hamster model of COVID-19. Nat Commun.
595 2021;12(1):5469.
596 61. Koenig PA, Das H, Liu H, Kummerer BM, Gohr FN, Jenster LM, et al. Structure-guided multivalent
597 nanobodies block SARS-CoV-2 infection and suppress mutational escape. Science. 2021;371(6530).
598 62. Pinto D, Park YJ, Beltramello M, Walls AC, Tortorici MA, Bianchi S, et al. Cross-neutralization of
599 SARS-CoV-2 by a human monoclonal SARS-CoV antibody. Nature. 2020;583(7815):290-5.
600 63. CDC. FDA updates Sotrovimab emergency use authorization (04/05/2022) 2022 [Available from:
601 https://www.fda.gov/drugs/drug-safety-and-availability/fda-updates-sotrovimab-emergency-use-
602 authorization.
603 64. Grange ZL, Goldstein T, Johnson CK, Anthony S, Gilardi K, Daszak P, et al. Ranking the risk of
604 animal-to-human spillover for newly discovered viruses. Proc Natl Acad Sci U S A. 2021;118(15).
605 65. Xiang Y, Nambulli S, Xiao Z, Liu H, Sang Z, Duprex WP, et al. Versatile and multivalent nanobodies
606 efficiently neutralize SARS-CoV-2. Science. 2020;370(6523):1479-84.
607 66. Kumar S, Stecher G, Li M, Knyaz C, Tamura K. MEGA X: Molecular Evolutionary Genetics Analysis
608 across Computing Platforms. Mol Biol Evol. 2018;35(6):1547-9.
609 67. Chao G, Lau WL, Hackel BJ, Sazinsky SL, Lippow SM, Wittrup KD. Isolating and engineering
610 human antibodies using yeast surface display. Nat Protoc. 2006;1(2):755-68.
611 68. Xu C, Wang Y, Liu C, Zhang C, Han W, Hong X, et al. Conformational dynamics of SARS-CoV-2
612 trimeric spike glycoprotein in complex with receptor ACE2 revealed by cryo-EM. Sci Adv. 2021;7(1).

613

614

615

616

617

618

619

620

621

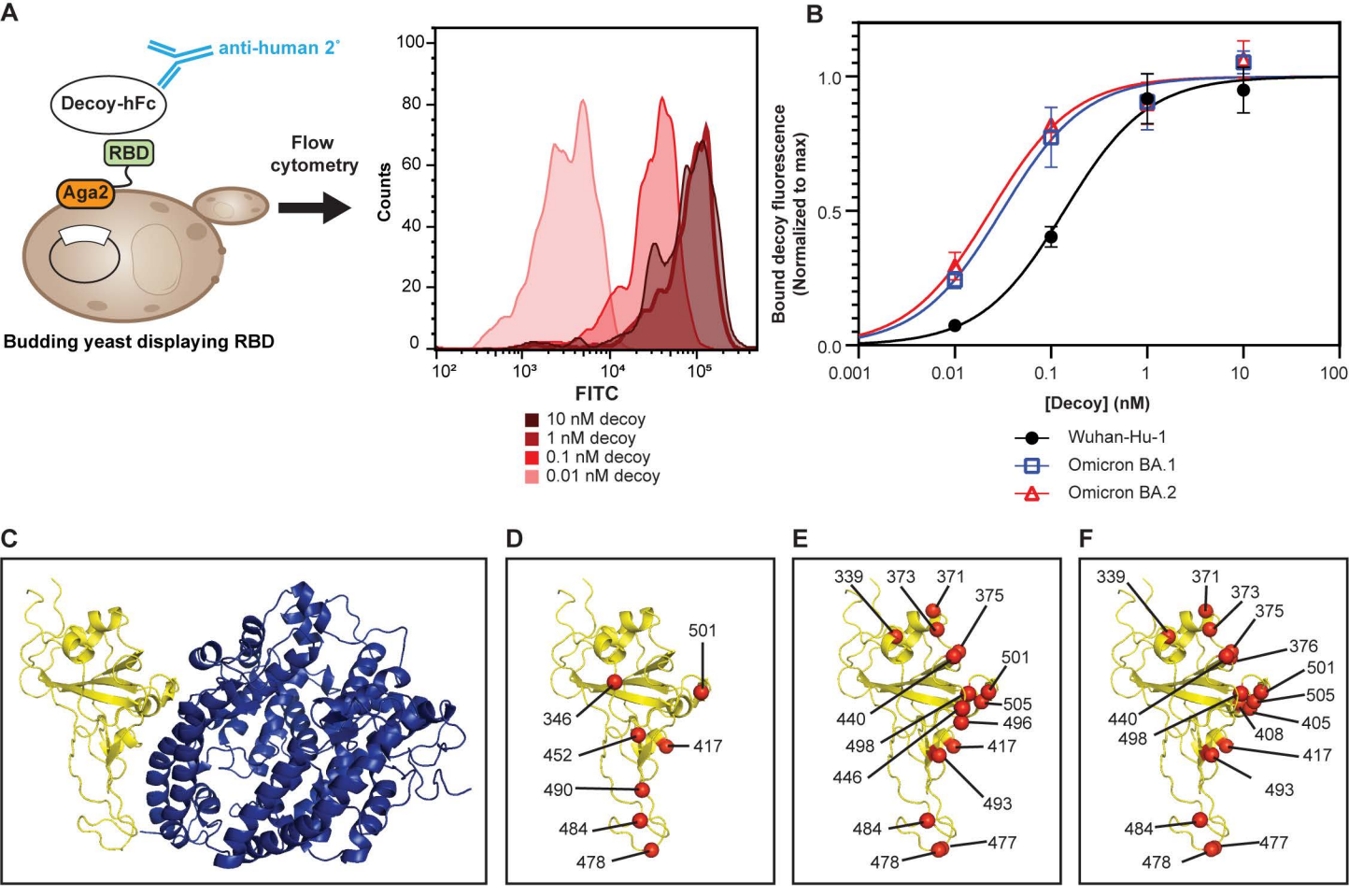
A
anti-human 2°
Decoy-hFc
RBD
Aga2
Budding yeast displaying RBD
Flow cytometry
Counts
FITC
10 nM decoy
1 nM decoy
0.1 nM decoy
0.01 nM decoy
B
Bound decoy fluorescence (Normalized to max)
[Decoy] (nM)
Wuhan-Hu-1
Omicron BA.1
Omicron BA.2
C
D
E
F

622 **Figure Captions**

623 **Fig 1. CDY14HL maintains tight binding to diverse SARS-CoV-2 variants**

624 (A) Scheme for measuring decoy binding to yeast surface-expressed RBDs. Histograms are from
625 a representative replicate of decoy binding to yeast-displayed Wuhan-Hu-1 RBD. (B)
626 Representative decoy binding data for the RBD from the ancestral (Wuhan-Hu-1) SARS-CoV-2
627 strain and both Omicron variants. (C) The complex (68) between the SARS-CoV-2 Wuhan-Hu-
628 1 RBD (yellow ribbons) and human ACE2 (blue ribbons). (D) The Wuhan-Hu-1 RBD from the
629 ACE2 complex structure is shown alone. Red spheres indicate the α-carbon of amino acid
630 residues mutated in several pre-Omicron SARS-CoV-2 variant strains. Amino acid position
631 numbers are show for each mutated residue. These mutations cluster around the interface with
632 ACE2. Wuhan-Hu-1 RBD is shown with the positions mutated in Omicron BA.1 (E) and
633 Omicron.BA.2 (F) in red spheres.Error bars represent standard deviation of at least four replicate
634 measurements.

635

636

637

638

639

640

641

642

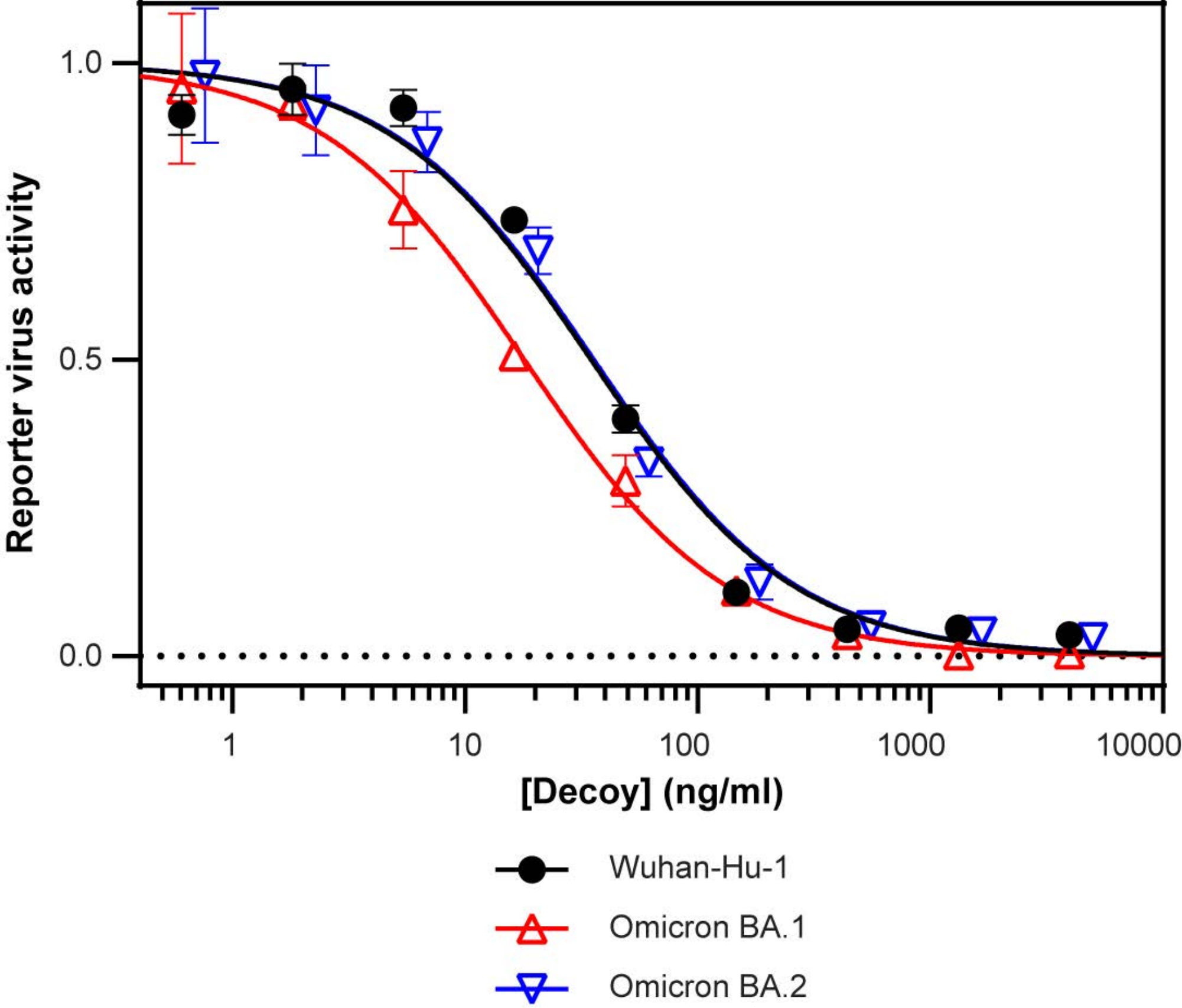
1.0
0.5
0.0
Reporter virus activity
1
10
100
1000
10000
[Decoy] (ng/ml)
Wuhan-Hu-1
Omicron BA.1
Omicron BA.2

643 **Fig 2. CDY14HL maintains potent neutralization for diverse SARS-CoV-2 variants**

644 Viral neutralization assay using lentiviruses pseudotyped with the ancestral (Wuhan-Hu-1),
645 Omicron BA.1, or Omicron BA.2 variant spike protein. Error bars represent standard deviation
646 of at least three replicate measurements.

647

648

649

650

651

652

653

654

655

656

657

658

659

660

661

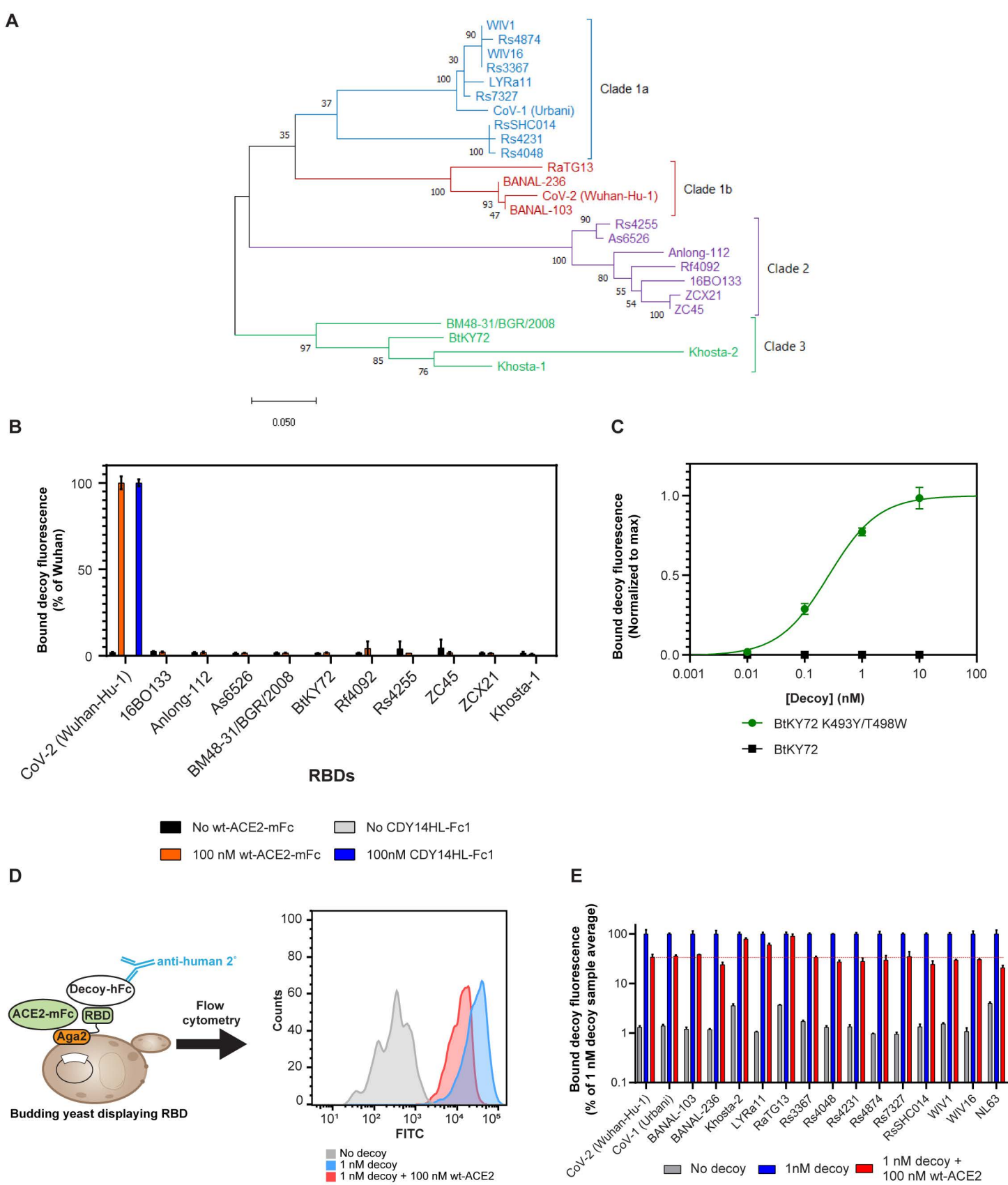
A
WIV1
Rs4874
WIV16
Rs3367
LYRa11
Rs7327
CoV-1 (Urbani)
RsSHC014
Rs4231
Rs4048
Clade 1a
RaTG13
BANAL-236
CoV-2 (Wuhan-Hu-1)
BANAL-103
Clade 1b
Rs4255
As6526
Anlong-112
Rf4092
16BO133
ZCX21
ZC45
Clade 2
BM48-31/BGR/2008
BtKY72
Khosta-2
Khosta-1
Clade 3
0.050
B
Bound decoy fluorescence (% of Wuhan)
CoV-2 (Wuhan-Hu-1)
16BO133
Anlong-112
As6526
BM48-31/BGR/2008
BtKY72
Rf4092
Rs4255
ZC45
ZCX21
Khosta-1
RBDs
No wt-ACE2-mFc
100 nM wt-ACE2-mFc
No CDY14HL-Fc1
100nM CDY14HL-Fc1
C
Bound decoy fluorescence (Normalized to max)
[Decoy] (nM)
BtKY72 K493Y/T498W
BtKY72
D
anti-human 2°
Decoy-hFc
ACE2-mFc
RBD
Aga2
Budding yeast displaying RBD
Flow cytometry
Counts
FITC
No decoy
1 nM decoy
1 nM decoy + 100 nM wt-ACE2
E
Bound decoy fluorescence (% of 1 nM decoy sample average)
CoV-2 (Wuhan-Hu-1)
CoV-1 (Urbani)
BANAL-103
BANAL-236
Khosta-2
LYRa11
RaTG13
Rs3367
Rs4048
Rs4231
Rs4874
Rs7327
RsSHC014
WIV1
WIV16
NL63
No decoy
1nM decoy
1 nM decoy + 100 nM wt-ACE2

662 **Fig 3. CDY14HL binds diverse ACE2-dependent CoVs**

663 (A) Phylogenetic tree of *sarbecovirus* RBDs created using the maximum likelihood method. (B)
664 Yeast displayed RBDs were used to test for decoy or wt-ACE2 binding at 100 nM. (C) Yeast
665 displayed BtKY72 RBDs were titrated with decoy and evaluated to determine the dissociation
666 equilibrium constant. (D) Schematic for measuring the competition between decoy and
667 endogenous ACE2 receptor using yeast-displayed RBDs. Histogram data are from a
668 representative replicate for the SARS-CoV-2 Wuhan-Hu-1 RBD. (E) Relative levels of decoy
669 binding to diverse RBDs under several conditions, as assessed via the yeast display system. Error
670 bars represent standard deviation of at least three replicate measurements.

Supplemental Materials

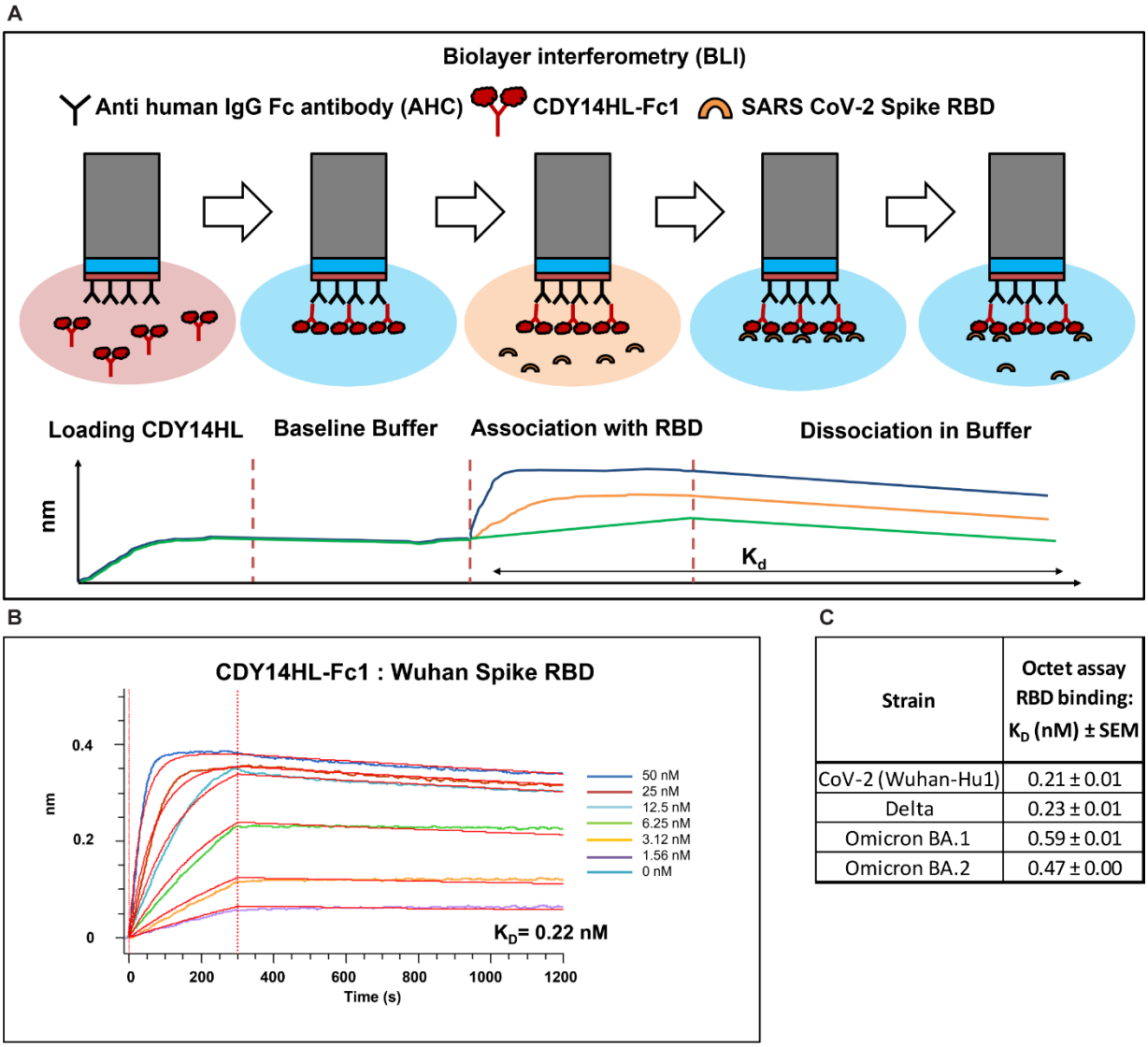

C

Strain	Octet assay RBD binding: K_D (nM) ± SEM
CoV-2 (Wuhan-Hu1)	0.21 ± 0.01
Delta	0.23 ± 0.01
Omicron BA.1	0.59 ± 0.01
Omicron BA.2	0.47 ± 0.00

Figure S1. *Biolayer interferometry (BLI) kinetics for CDY14HL-Fc1 and SARS-CoV-2 Variants*. **A)** Depiction of Biolayer interferometry assay format. CDY14HL-Fc1 was immobilized as ligand and SARS-CoV-2 variant RBD was used as analyte **B)** Representative fitted sensogram for CDY14HL-Fc1 and CoV-2 Wuhan-Hu-1 spike RBD **C)** Table of K_D values (nM) for CDY14HL-Fc1 and four SARS-CoV-2 variant RBDs. Mean values and standard error of the mean (SEM) determined from three technical replicates.

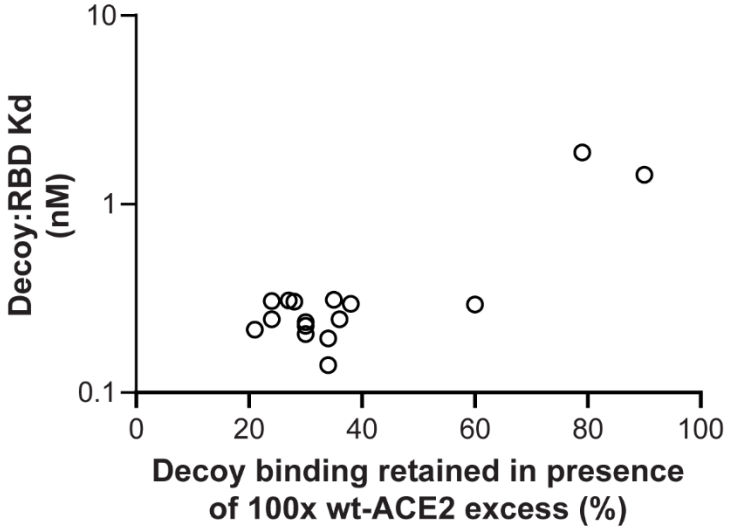

Figure S2. We use the data sets generated in **Table 2** and **Figure 3E** to evaluate the relationship between decoy affinity and the amount of decoy retained in a competitive binding assay.

Materials and Methods

Biolayer Interferometry

For the determination of binding affinity, biolayer interferometry measurements were taken on the Octet HTX (Sartorius Corporation). Purified CDY14HL-Fc1 was immobilized on an anti-human IgG Fc sensor (AHC sensor, Sartorius Corporation). Decoy loaded tips were dipped into wells containing purified His-tagged SARS-CoV-2 Spike RBD proteins (R&D Biotechne Corporation). RBD concentrations of 50, 25, 12.5, 6,25, 3.125 and 1.56 nM were used to determine the K_Ds. The diluent and running buffer for all experiments was 1x Kinetics Buffer (FortéBio, PBS+ 0.02% Tween20, 0.1% BSA, 0.05% sodium azide). K_D fits were determined by 1:1 binding model global grouped fits on the Octet Data Analysis HT Version 12.0.2.59 (FortéBio). All measurements were conducted in triplicate.

Plasmid and sequence details for constructs used in the main text

Nucleotide sequence of CDY14HL-Fc1:

ATGTCAAGCTCTTCCTGGCTCCTTCTCAGCCTTGTTGCTGTAACTGCTGCTCAGTCCA
CCATTGAGGAACAGGCCAAGACATTTTTGGACAtGTTTAACCACaAAGCCGAAGACC
TGTTCTATCAAAGTTCACTTGCTgCTTGGAATTATAACACCAATATTACTGAAGAGAA
TGTCCAAAACATGAATAAcGCTGGGGACAAATGGTCTGCCTTTTTAAAGGAACAGTC
CACAtTTGCCCAAATGTATCCACTACAAGAAATTCAGAATCcCACAGTCAAGCTTCAG
CTGCAGGCTCTTCAGCAAAATGGGTCTTCAGTGCTCTCAGAAGACAAGAGCAAACG
GTTGAACACAATTCTAAATACAATGAGCACCATCTACAGTACTGGAAAAGTTTGTAA
CCCgGATAATCCACAAGAATGCTTATTACTTGAACCAGGTTTGAATGAAATAATGGC
AAACAGTTTAGACTACAATGAGAGGCTCTGGGCTTGGGAAAGCTGGAGATCTGAGG
TCGGCAAGCAGCTGAGGCCATTATATGAAGAGTATGTGGTCTTGAAAAATGAGATG
GCgAGAGCAAAcCATTATGAGGACTATGGGGATTATTGGAGAGGAGACTATGAAGT
AAATGGGGTAGATGGCTATGACTACAGCCGCGGCCAGTTGATTGAAGATGTGGAAC
ATACCTTTGAAGAGATTAAACCATTATATGAACATCTTCATGCCTATGTGAGGGCAA
AGTTGATGAATGCCTATCCTTCCTATATCAGTCCAATTGGATGCCTCCCTGCTCATTT
GCTTGGTGATATGTGGGGTAGATTTTGGACAAATCTGTACTCTTTGACAGTTCCCTTc
GGACAGAAACCAAACATAGATGTTACTGATGCAATGGTGGACCAGGCCTGGGATGC
ACAGAGAATATTCAAGGAGGCCGAGAAGTTCTTTGTATCTGTTGGTCTTCCTAATAT
GACTCAAGGATTCTGGGAAtATTCCATGCTAACGGACCCAGGAAATGTTCAGAAAGC
AGTCTGCCtTCCCACAGCTTGGGACCTGGGGAAGGGCGACTTCAGGATCCTTATGTG
CACAAAGGTGACAATGGACGACTTCCTGACAGCTCATCATGAGATGGGGCATATCC
AGTATGATATGGCATATGCTGCACAACCTTTTCTGCTAAGAAATGGAGCTAATGAAG
GATTCCATGAAGCTGTTGGGGAAATCATGTCACTTTCTGCAGCCACACCTAAGCATT
TAAAATCCATTGGTCTTCTGTCACCCGATTTTCAAGAAGACAATGAAACAGAAATAA
ACTTCCTGCTCAAACAAGCACTCACGATTGTTGGGACTCTGCCATTTACTTACATGTT
AGAGAAGTGGAGGTGGATGGTCTTTAAAGGGGAAATTCCCAAAGACCAGTGGATGA
AAAAGTGGTGGGAGATGAAGCGAGAGATAGTTGGGGTGGTGGAACCTGTGCCCCAT
GATGAAACATACTGTGACCCCGCATCTCTGTTCCATGTTTCTAATGATTACTCATTCA
TTCGATATTACACAAGGACCCTTTACCAATTCCAGTTTCAAGAAGCACTTTGTCAAG

CAGCTAAACATGAAGGCCCTCTGCACAAATGTGACATCTCAAACTCTACAGAAGCT
GGACAGAAACTGTTCAATATGCTGAGGCTTGGAAAATCAGAACCCTGGACCCTAGC
ATTGGAAAATGTTGTAGGAGCAAAGAACATGAATGTAAGGCCACTGCTCAACTACT
TTGAGCCCTTATTTACCTGGCTGAAAGACCAGAACAAGAATTCTTTTGTGGGATGGA
GTACCGACTGGAGTCCATATGCAGACggaagtGACAAGACCCACACCTGTCCTCCATGT
CCTGCTCCAGAACTGCTCGGCGGACCTTCCGTGTTCCTGTTTCCTCCAAAGCCTAAG
GACACCCTGATGATCAGCAGAACCCCTGAAGTGACCTGCGTGGTGGTGGATGTGTCC
CACGAGGATCCCGAAGTGAAGTTCAATTGGTACGTGGACGGCGTGGAAGTGCACAA
CGCCAAGACCAAGCCTAGAGAGGAACAGTACAACAGCACCTACAGAGTGGTGTCCG
TGCTGACCGTGCTGCACCAGGATTGGCTGAACGGCAAAGAGTACAAGTGCAAGGTG
TCCAACAAGGCCCTGCCTGCTCCTATCGAGAAAACCATCAGCAAGGCCAAGGGCCA
GCCTAGGGAACCCCAGGTTTACACACTGCCTCCAAGCAGGGACGAGCTGACCAAGA
ATCAGGTGTCCCTGACCTGCCTCGTGAAGGGCTTCTACCCTTCCGATATCGCCGTGG
AATGGGAGAGCAACGGCCAGCCTGAGAACAACTACAAGACAACCCCTCCTGTGCTG
GACAGCGACGGCTCATTCTTCCTGTACAGCAAGCTGACAGTGGACAAGTCCAGGTG
GCAGCAGGGCAACGTGTTCAGCTGCAGCGTGATGCACGAGGCCCTGCACAACCACT
ACACCCAGAAGTCCCTGAGCCTGTCTCCTGGAaaaTGATGA

Nucleotide sequence of wt-ACE2-mFc (human ACE2 1-615 fused to Fc from mouse IgG2A)

ATGTCAAGCTCTTCCTGGCTCCTTCTCAGCCTTGTTGCTGTAACTGCTGCTCAGTCCA
CCATTGAGGAACAGGCCAAGACATTTTTGGACAAGTTTAACCACGAAGCCGAAGAC
CTGTTCTATCAAAGTTCACTTGCTTCTTGGAATTATAACACCAATATTACTGAAGAG
AATGTCCAAAACATGAATAATGCTGGGGACAAATGGTCTGCCTTTTTAAAGGAACA
GTCCACACTTGCCCAAATGTATCCACTACAAGAAATTCAGAATCTCACAGTCAAGCT
TCAGCTGCAGGCTCTTCAGCAAAATGGGTCTTCAGTGCTCTCAGAAGACAAGAGCA
AACGGTTGAACACAATTCTAAATACAATGAGCACCATCTACAGTACTGGAAAAGTTT
GTAACCCAGATAATCCACAAGAATGCTTATTACTTGAACCAGGTTTGAATGAAATAA
TGGCAAACAGTTTAGACTACAATGAGAGGCTCTGGGCTTGGGAAAGCTGGAGATCT
GAGGTCGGCAAGCAGCTGAGGCCATTATATGAAGAGTATGTGGTCTTGAAAAATGA
GATGGCAAGAGCAAATCATTATGAGGACTATGGGGATTATTGGAGAGGAGACTATG
AAGTAAATGGGGTAGATGGCTATGACTACAGCCGCGGCCAGTTGATTGAAGATGTG
GAACATACCTTTGAAGAGATTAAACCATTATATGAACATCTTCATGCCTATGTGAGG
GCAAAGTTGATGAATGCCTATCCTTCCTATATCAGTCCAATTGGATGCCTCCCTGCTC
ATTTGCTTGGTGATATGTGGGGTAGATTTTGGACAAATCTGTACTCTTTGACAGTTCC
CTTTGGACAGAAACCAAACATAGATGTTACTGATGCAATGGTGGACCAGGCCTGGG
ATGCACAGAGAATATTCAAGGAGGCCGAGAAGTTCTTTGTATCTGTTGGTCTTCCTA
ATATGACTCAAGGATTCTGGGAAAATTCCATGCTAACGGACCCAGGAAATGTTCAG
AAAGCAGTCTGCCATCCCACAGCTTGGGACCTGGGGAAGGGCGACTTCAGGATCCT
TATGTGCACAAAGGTGACAATGGACGACTTCCTGACAGCTCATCATGAGATGGGGC
ATATCCAGTATGATATGGCATATGCTGCACAACCTTTTCTGCTAAGAAATGGAGCTA
ATGAAGGATTCCATGAAGCTGTTGGGGAAATCATGTCACTTTCTGCAGCCACACCTA
AGCATTTAAAATCCATTGGTCTTCTGTCACCCGATTTTCAAGAAGACAATGAAACAG

AAATAAACTTCCTGCTCAAACAAGCACTCACGATTGTTGGGACTCTGCCATTTACTT
ACATGTTAGAGAAGTGGAGGTGGATGGTCTTTAAAGGGGAAATTCCCAAAGACCAG
TGGATGAAAAAGTGGTGGGAGATGAAGCGAGAGATAGTTGGGGTGGTGGAACCTGT
GCCCCATGATGAAACATACTGTGACCCCGCATCTCTGTTCCATGTTTCTAATGATTAC
TCATTCATTCGATATTACACAAGGACCCTTTACCAATTCCAGTTTCAAGAAGCACTTT
GTCAAGCAGCTAAACATGAAGGCCCTCTGCACAAATGTGACATCTCAAACTCTACA
GAAGCTGGACAGAAACTGTTCAATATGCTGAGGCTTGGAAAATCAGAACCCTGGAC
CCTAGCATTGGAAAATGTTGTAGGAGCAAAGAACATGAATGTAAGGCCACTGCTCA
ACTACTTTGAGCCCTTATTTACCTGGCTGAAAGACCAGAACAAGAATTCTTTTGTGG
GATGGAGTACCGACTGGAGTCCATATGCAGACCCCAGAGGGCCCACAATCAAGCCC
TGTCCTCCATGCAAATGCCCAGCACCTAACCTCTTGGGTGGACCATCCGTCTTCATCT
TCCCTCCAAAGATCAAGGATGTACTCATGATCTCCCTGAGCCCCATAGTCACATGTG
TGGTGGTGGATGTGAGCGAGGATGACCCAGATGTCCAGATCAGCTGGTTTGTGAAC
AACGTGGAAGTACACACAGCTCAGACACAAACCCATAGAGAGGATTACAACAGTAC
TCTCCGGGTGGTCAGTGCCCTCCCCATCCAGCACCAGGACTGGATGAGTGGCAAGG
AGTTCAAATGCAAGGTCAACAACAAAGACCTCCCAGCGCCCATCGAGAGAACCATC
TCAAAACCCAAAGGGTCAGTAAGAGCTCCACAGGTATATGTCTTGCCTCCACCAGA
AGAAGAGATGACTAAGAAACAGGTCACTCTGACCTGCATGGTCACAGACTTCATGC
CTGAAGACATTTACGTGGAGTGGACCAACAACGGGAAAACAGAGCTAAACTACAAG
AACACTGAACCAGTCCTGGACTCTGATGGTTCTTACTTCATGTACAGCAAGCTGAGA
GTGGAAAAGAAGAACTGGGTGGAAAGAAATAGCTACTCCTGTTCAGTGGTCCACGA
GGGTCTGCACAATCACCACACGACTAAGAGCTTCTCCCGGACTCCGGGTAAATGA

Map of typical Aga2-RBD-HA construct used for yeast display

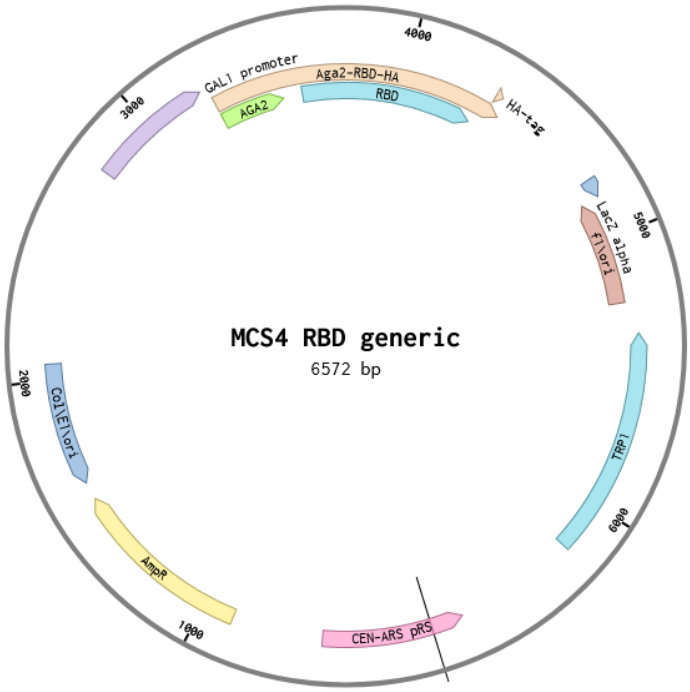

Sequence of Aga2-Wuhan-Hu-1-RBD-HA

ATGCAGTTACTTCGCTGTTTTTCAATATTTTCTGTTATTGCTTCAGTTTTAGCACAGG
AACTGACAACTATATGCGAGCAAATCCCCTCACCAACTTTAGAATCGACGCCGTACT
CTTTGTCAACGACTACTATTTTGGCCAACGGGAAGGCAATGCAAGGAGTTTTTGAAT
ATTACAAATCAGTAACGTTTGTCAGTAATTGCGGTTCTCACCCCTCAACAACTAGCA
AAGGCAGCCCCATAAACACACAGTATGTTTTTAAGGACAATAGCTCGACGATTGAA
GGTAGAGGATCCGGAGGTAGCGGATCAGGAGGTGGAGGCTCCGGAGGAGGTGGAC
CAAACATCACCAATCTGTGCCCCTTCGGCGAAGTTTTCAACGCCACCAGATTCGCCA
GCGTGTACGCCTGGAATAGAAAGCGGATCAGCAACTGTGTGGCCGACTACAGCGTG
CTGTATAACAGCGCCAGCTTCAGCACATTCAAGTGCTACGGCGTGTCCCCTACCAAG
CTGAACGACCTGTGTTTTACCAACGTGTACGCCGATAGCTTCGTGATTAGAGGCGAC
GAGGTGCGGCAGATCGCCCCTGGCCAGACCGGTAAGATCGCTGATTACAACTACAA
GCTGCCTGACGACTTCACCGGCTGTGTGATCGCCTGGAACAGCAACAACCTGGACA
GCAAGGTGGGCGGCAACTATAACTACCTGTACCGGCTGTTCAGAAAATCTAATCTGA
AGCCCTTCGAGAGAGATATCAGCACAGAGATCTACCAGGCCGGCAGCACCCCTTGC
AACGGCGTGGAAGGCTTTAACTGCTACTTCCCCCTGCAGAGCTACGGATTCCAGCCA
ACAAATGGAGTCGGCTACCAACCTTACAGAGTGGTCGTGCTCTCCTTTGAGCTGCTG
CACGCCCCTGCCACAGTGTGCGGACCTAAGAAAAGCGGATCTTCTGGATCTGGATCT
GGATCTGAATCTAAGTCTACTGGATACCCATACGACGTTCCAGACTACGCTCTGCAG
GCTAGTGGTTGA